ACS APPLIED MATERIALS & INTERFACES
Research Article
www.acsami.org

Facile Size-Tunable Fabrication of Functional Tin Dioxide Nanostructures by Multiple Size Reduction Lithography

Hyeong-Ho Park,[†] Wai Lung Law,[‡,§] Xin Zhang,[⊥,‡] Seon-Yong Hwang,[†] Sang Hyun Jung,[†] Hyun-Beom Shin,[†] Ho Kwan Kang,*[,†] Hyung-Ho Park,[∥] Ross H. Hill,[⊥,‡] and Chul Ki Ko[†]

[†]Patterning Process Department, Nano Process Division, Korea Advanced Nano Fab Center (KANC), Suwon 443-270, Republic of Korea

[⊥]4D LABS and [‡]Department of Chemistry, Simon Fraser University, Burnaby, British Columbia V5A 1S6, Canada

[∥]Department of Materials Science and Engineering, Yonsei University, Seoul 120-749, Republic of Korea

Supporting Information

ABSTRACT: A novel ultraviolet (UV)-assisted imprinting procedure that employs photosensitive tin(II) 2-ethylhexanoate is presented for the facile size-tunable fabrication of functional tin dioxide (SnO_2) nanostructures by varying annealing temperatures. These imprinted SnO_2 nanostructures were also used as new masters for size reduction lithography. SnO_2 lines down to 40 nm wide were obtained from a silicon master with 200 nm wide lines by simply performing size reduction lithography twice. This leads to 80 and 87.5% reduction in the width and height of imprinted lines, respectively. An imprinted pattern annealed at 400 °C demonstrated transmittance greater than 90% over the range of 350−700 nm, which is high enough to make the pattern useful as a transparent SnO_2 mold. This demonstrated approach allows the accessibility to size-tunable molds, eliminating the need for conventional expensive imprinting masters with very fine structures, as well as functional SnO_2 nanostructures, potentially useful in applications where ordered surface nanostructures are required, such as photonic crystals, biological sensors, and model catalysts.

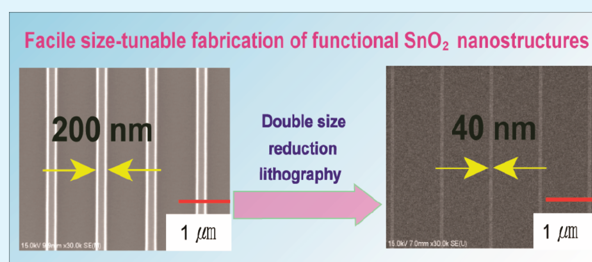

KEYWORDS: *tin dioxide, photochemical mechanism, nanoimprint lithography, size reduction lithography*

INTRODUCTION

Great effort has been expended on developing facile techniques to fabricate periodic nanostructures because of their potential applications in photonic crystals, biological sensors, and model catalysts.[1−6] Several techniques capable of fabricating sub-50-nm nanostructures have involved the use of top-down nanolithography such as focused ion beam (FIB) lithography and electron beam lithography (EBL).[7,8] These techniques are expensive and limited by a trade-off between resolution and throughput. In contrast, unconventional techniques such as nanoimprint lithography (NIL) and soft lithography are simple to operate, cost-effective, and suitable for large-area patterning.[9−11] For NIL, there are two major processing approaches, thermal-NIL (T-NIL) and ultraviolet-NIL (UV-NIL), each of which is applicable to a special type of resist materials.[10,11] T-NIL, employing thermoplastic polymers, suffers from low throughput due to the need of holding the process at an elevated temperature to induce thermal reaction of the thermoplastic polymers. In addition, T-NIL is not suitable for continuous roll-to-roll NIL processes using a cylinder mold. Of the two NIL approaches, UV-NIL has a greater potential to overcome these limitations. Since UV-NIL is traditionally known as a one-to-one pattern replication process, each new imprint pattern requires a new imprint mold and often a new master for the mold. As a result of this, masters and molds for imprint lithography have become expensive consumables in the UV-NIL process. Therefore, searching for a cheaper and more convenient method to generate new nanoimprint masters and molds is necessary.

Research has been conducted in various directions to develop efficient size reduction techniques, in order to overcome the limitations of traditional lithography techniques. Size reduction lithography was first developed by Choi et al.[6,12] By coupling photolithography with chemical vapor deposition (CVD) and selective chemical etch, structures much smaller than normal diffraction limit of photolithography were obtained. Since a sacrificial CVD layer is used in the technique to reduce feature sizes, it is also called spacer lithography. By repeating spacer lithography multiple times, sub-10 nm structures were demonstrated.[6] Low et al. reported the use of a "mix and match" sequential imprinting technique, where line-space patterns of different gap sizes were obtained by varying combinations of feature size and relative alignment of imprinting molds.[13] In our previous work, we demonstrated

Received: February 6, 2012
Accepted: April 4, 2012
Published: April 4, 2012

 © 2012 American Chemical Society

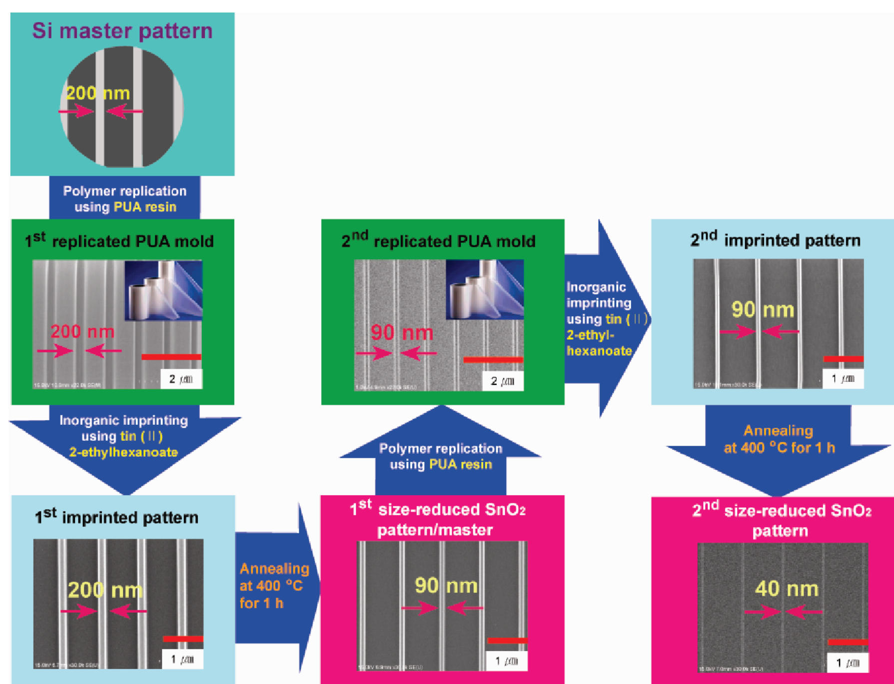

Figure 1. Schematic diagram of the novel double size reduction lithography using a poly(urethaneacrylate) resin and photosensitive tin(II) 2-ethylhexanoate.

the facile fabrication of both amorphous and crystalline ZrO_2 nanostructures by direct UV-NIL process using a photosensitive Zr-containing metal–organic compound.[14] It was found that the feature size of directly patterned ZrO_2 nanostructures can be tuned by varying the annealing temperature. We anticipated that it would be worthwhile to apply this method to the fabrication of various replicated tin oxide patterns and polymer molds with reduced feature sizes, using a photosensitive tin-containing metal–organic compound and a poly(urethaneacrylate) (PUA) resin.

Tin dioxide (SnO_2) is of great importance due to its wide range of applications. SnO_2 can be used as a catalyst, gas sensors, transparent electrodes in display devices, and an anode material in lithium-ion batteries.[15−18] Recently, of great interest is nanostructured SnO_2, whose properties could be significantly improved in comparison with its bulk material benefiting from nanometer size effects.[19,20] However, because of its high chemical durability,[21,22] fine patterning of SnO_2 films by wet chemical etch is rather complicated. In our UV-NIL process, a photosensitive tin-containing metal–organic compound is used for the nanofabrication of functional SnO_2 films to avoid wet chemical etch.

In this work, we demonstrate the use of a sequential polymer PUA replication and metal–organic precursor imprinting process to fabricate various PUA molds and imprinted nanostructures, where the feature size can be greatly reduced by annealing the imprinted nanostructures and further repeating the sequential fabrication process. This method provides us with a novel way to reduce the feature size without the need to fabricate new masters, as the imprinted and annealed SnO_2 structures can be used as masters for making new PUA molds. Photochemical reaction of the tin-containing compound used in the process, and optical band gap, optical transmittance, and refractive index of imprinted and annealed SnO_2 films are also investigated. In addition, the electrical properties such as the resistivity and carrier concentration of the functional SnO_2 materials are studied, as the UV-NIL technique described here can be potentially useful for fabricating patterns of transparent conducting oxides (TCOs).

EXPERIMENTAL SECTION

Fabrication of Polymer PUA Molds and SnO_2 Nanostructures/Masters. The silicon master used in this paper consists of line-space gratings of 1000 nm pitch, where the lines are 200 nm wide and 400 nm high, fabricated by deep ultraviolet (DUV) lithography and subsequent deep reactive ion etching. Structures on the silicon master were replicated onto a PUA mold as a first replicated PUA mold by UV imprinting to obtain a flexible polymer mold as described elsewhere.[23,24] Images of the silicon master and first replicated PUA mold can be found in Figure 1. Prior to use for imprinting, the PUA mold was treated by vapor phase deposition of trichloro(1H, 1H, 2H-2H-perfluorootyl)silane (97%, Sigma-Aldrich Co.) to improve the release between the PUA mold and the film to be imprinted.[25]

The precursor (i.e., photosensitive tin-containing metal–organic compound) used for imprinting SnO_2 nanostructures was tin(II) 2-ethylhexanoate (Alfa Aesar). To prepare a precursor solution for spin-coating, we dissolved tin(II) 2-ethylhexanoate in hexane (Sigma Aldrich) at a concentration of 0.3 M. The solution was filtered with a syringe through a 0.45-μm poly(tetrafluoroethylene) (PTFE) membrane. A silicon substrate, p-Si (100) (LG Siltron), was immersed in an acetone bath under sonication for 5 min, followed by an immersion in isopropyl alcohol for 5 min, and then rinsed with deionized (DI) water (Milli-Q, Millipore Corp.) for 3 min. The substrate was dried under a nitrogen flow and further treated with argon plasma in a plasma cleaner (PDC-002, Harrick Scientific Corp.) for 5 min. The cleaned silicon substrate was treated with an adhesion promoter, Exfix (ZAP-1020, ChemOptics), to enhance the adhesion between the silicon substrate and the spin-coated film. This was accomplished by spin-coating the adhesion promoter onto the silicon substrate at 3000 rpm for 60 s, followed by heating the substrate on a hot plate at 110 °C for 2 min. The thickness of the spin-coated Exfix films was a few tens of angstroms (Å). A photosensitive precursor film was prepared by spin-coating the above solution of tin(II) 2-ethylhexanoate onto the promoter-treated silicon substrate at 1500 rpm for 60 s. The film was baked on a hot plate at 80 °C for 3 min to

remove residual solvent in the film. The first replicated PUA mold was then pressed against the film at a pressure of 6 bar at room temperature for 5 min, using a NIL-8 imprinter (Obducat, Sweden). The film was exposed to UV light (25 mW cm^{-2} with a major wavelength peak of 365 nm) through the PUA mold for 20 min to induce a photochemical reaction. By detaching the PUA mold from the irradiated film, a first imprinted tin-containing pattern was obtained. To reduce the feature size, the first imprinted pattern was annealed at 400 °C for 1 h in air. Images of both the as-imprinted and annealed patterns can be found in Figure 1. The annealed SnO_2 pattern was then used as a new master to replicate structures onto a second replicated PUA mold. The second replicated PUA mold is utilized to repeat above imprinting and annealing steps on a second photosensitive precursor film, to further reduce the feature size. A schematic diagram of the above size reduction lithography, where the PUA mold fabrication and the metal−organic-compound imprinting and annealing processes are performed twice, is presented in Figure 1.

Characterization Methods. Fourier transform infrared spectroscopy (FTIR) was conducted using a Jasco 300Z spectrometer to monitor the photochemical reaction of a tin-containing precursor film. Imprinted and annealed tin-containing nanostructures were examined using a PSIA XE-100 atomic force microscope operated in noncontact mode and a Hitachi S-4800 field-emission scanning electron microscope. The optical transmission and absorbance measurements were performed in the range of 200−1000 nm by a Varian Cary 5000 ultraviolet−visible−near-infrared (UV−vis−NIR) spectrophotometer. The absorption coefficients α for the tin-containing films were determined from the measured absorbance (A) using the following equation[26]

$$\alpha = (A \ln 10)/d \qquad (1)$$

where d is the film thickness (cm). The thickness and refractive index of the films were measured with a spectroscopic ellipsometer (Model ELLI-SE(UV)-FM6-R, Ellipso Technology) at an incidence angle of 70°. The crystallinity of UV-irradiated and annealed SnO_2 films was investigated by X-ray diffraction using a Rigaku D/Max 2500 diffractometer with Cu K_α radiation (λ = 1.54178 Å), operated at 40 kV and 300 mA. The electrical properties of the films were measured using a Bio-Rad HL5500PC Hall system with probes placed on samples in the van der Pauw geometry.

RESULTS AND DISCUSSION

FTIR was used to study the photochemical reaction of tin(II) 2-ethylhexanoate during UV irradiation. A precursor film of the compound was prepared on a Si wafer using the aforementioned spin-coating procedure. The FTIR spectrum of the film, in the range of 1000−3500 cm^{-1}, was collected as shown by Figure 2. The absorption bands at 2960, 2940, and 2865 cm^{-1} were assigned to antisymmetric and symmetric stretching vibrations of alkyl ($-CH_3$) and alkene ($-CH_2$) groups.[27] The absorption band at 1709 cm^{-1} is associated with carbonyl stretching vibration of free 2-ethylhexanoaic acid. The absorption bands at 1610 and 1562 cm^{-1} are associated with antisymmetric vibrations of carboxylate ($-CO_2-$) groups and those at 1462 and 1418 cm^{-1} are associated with symmetric vibrations of carboxylate ($-CO_2-$) groups. The frequency difference between the antisymmetric and symmetric stretching vibrations of ($-CO_2-$) groups in a metal carboxylate is known to correlate to the binding modes (i.e., bidentate, bridging, and unidentate) of the carboxylate ligands.[28] Here, two frequency differences, 100 and 192 cm^{-1} that are close to the typical values for bidentate and bridging modes, are observed for tin(II) 2-ethylhexanoate, indicating the presence of both bidentate and bridging 2-ethylhexanoate ligands. The absorption bands between 1320 and 1200 cm^{-1} are due to the vibrations of hydrocarbon chains ($-CH_2-$).[27] The film was then exposed to UV irradiation, and FTIR spectra of the film

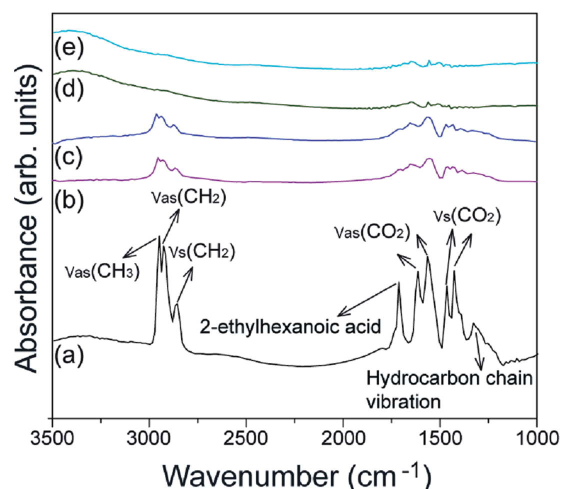

Figure 2. FTIR spectra of a precursor film spin-coated from tin(II) 2-ethylhexanoate collected at photolysis times of (a) 0, (b) 5, (c) 10, (d) 20, and (e) 30 min with 365 nm UV light.

were collected at various exposure times as shown in Figure 2. Upon UV exposure, the intensities of all the absorption bands associated with the organic groups in the film decreased, indicating decomposition of the precursor molecules and loss of organic groups in the film. These bands mostly disappeared after 20 min of UV exposure and extended UV exposure did not result in any further substantial change in FTIR spectrum, implying completion of the photochemical decomposition.

A film resulted from the complete photolysis of a tin(II) 2-ethylhexanoate film cast from hexane was examined by Auger electron spectroscopy (AES).[29] The results are summarized in Table 1. Tin, oxygen, and a small amount of carbon were

Table 1. AES data of the Film Produced by Photolysis of Tin(II) 2-Ethylhexanoate

sputter time (s)	%Sn	%O	%C
0	46 ± 3	40 ± 3	14 ± 6
12	51 ± 4	49 ± 5	0
24	51 ± 4	49 ± 2	0

observed from the surface of the film. By argon sputtering the film for 12 s, a carbon-free interior is revealed with an elemental ratio of Sn:O of 1:1, indicating that the carbon detected on the film surface is presumably due to absorption of carbon-containing contaminants. A further 12 s of argon sputtering resulted in a similar elemental composition. The AES results implied an elemental composition within the error of that of tin(II) oxide, SnO. Therefore, the photolysis of a precursor film of tin(II) 2-ethylhexanoate resulted in the loss of all organic ligands and the formation of tin(II) oxide.

To further understand the photolysis process, we investigated volatile photoproducts of tin(II) 2-ethylhexanoate by mass spectroscopy (MS) and the observed mass to charge ratios (m/z) and analyzed results are summarized in Table S1 in the Supporting Information.[29] A freshly prepared precursor film of tin(II) 2-ethylhexanoate on a Si chip was placed in a custom-made quartz cuvette, and the cuvette was evacuated and sealed to reduce influence from air. The film inside the evacuated cuvette was irradiated with a UV light for 20 min. The volatile photoproducts collected in the cuvette were then analyzed with a mass spectrometer. The highest mass/charge

peaks detected were at 100 and 98. These were presumably associated with the parent ions of heptane and heptene.[27,29] There was also an intense mass/charge peak observed at 44, associated with the molecular ions of carbon dioxide. A peak at 28 could be due to molecular ions of either CO from photoproducts, or N_2 from residual air. The remaining peaks were all assigned to various fragment ions of heptane and heptene. Combining the MS results with the FTIR and AES analyses, a photochemical decomposition mechanism was postulated for the photolysis of tin(II) 2-ethylhexanoate, as depicted in Figure 3. In Figure 3, the chainlike molecule *a* is a general formula proposed for tin(II) 2-ethylhexanoate to reflect the presence of both bidentate and bridging ligands. Here, R represents a heptyl group and *n* can be zero or a positive whole number. Because intensities of the absorption bands associated with bidentate and bridging ligands were similar, *n* is not expected to be very large. Presumably, tin(II) 2-ethylhexanoate in the precursor film formed small oligmeric molecules that contain a few tin(II) centers. Molecule *b* in Figure 3, the simplest molecular form containing both bidentate and bridging ligands, is used to interpret the photochemical decomposition of tin(II) 2-ethylhexanoate. During UV exposure, molecule *b* could absorb a photon and undergo a ligand-to-metal-charge-transfer (LMCT) transition, as indicated by the excited molecule *c*. This would result in a transfer of an electron from a 2-ethylhexanoate ligand to its linking tin(II) center. As a result, a Sn−O bond would break and a tin(I) center would be generated, as shown by species *d* in Figure 3. The excited molecule *c* and the species *d* illustrate a situation where a bridging ligand is involved in the LMCT process. The loss of an electron leads to fragmentation of the involved ligand, releasing a carbon dioxide and a heptyl radical and leaving species *e* a tin(I) center. The tin(I) center, with a thermally unfavorable oxidation state, causes further loss and fragmentation of the remaining ligands through two possible pathways, where the main difference lies in the fragmentation of 2-ethylhexanote ligands.[14,28−30] Through pathway A, all remaining ligands fragment in a fashion similar to the first fragmented ligand, and species *e* decomposes into Sn atoms, CO_2 molecules, and heptyl radicals. However, through pathway B, some of the remaining ligands fragment to form CO molecules, heptyl radicals, and leaving oxygen behind (highlighted in red in Figure 3). Therefore, species *e* decomposes into tin(II) oxide, CO and CO_2 molecules, and heptyl radicals. Regardless of the different photoproducts, both pathways lead to the complete loss of ligands from tin(II) 2-ethylhexanoate upon photolysis, which is consistent with our FTIR observation.

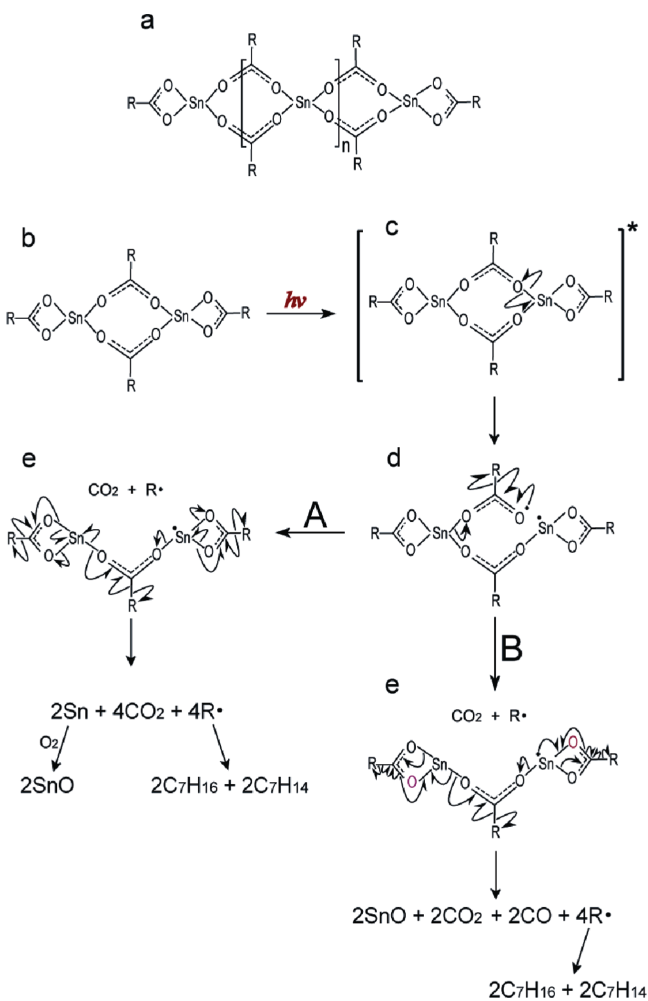

Figure 3. Proposed photolysis mechanism for tin(II) 2-ethylhexanoate.

When exposed to air, the reactive Sn atoms resulted from pathway A can be easily oxidized by oxygen in air, forming tin(II) oxide that is the same as the solid photoproduct resulted from pathway B. The composition of the photolyzed film was confirmed to be tin(II) oxide by AES analysis. A reactive heptyl radical can encounter another one and abstract a hydrogen from it, generating a heptane molecule and a heptene molecule.[28−30] The formation of CO, CO_2, heptane (C_7H_{16}), and heptene (C_7H_{14}) is consistent with the MS results. A bidentate ligand could also be involved in the LMCT process. In this case, the loss and fragmentation of ligands would start with the involved bidentate ligand. However, the further loss and fragmentation of remaining ligands are expected to follow a manner similar to the above-mentioned reaction pathways, resulting in the same photoproducts.

In summary, films of tin(II) 2-ethylhexanoate can be spin-cast from a precursor solution in hexane and these films are found to be photosensitive. UV exposure can result in the loss and fragmentation of 2-ethylhexanoate ligands in the precursor films. Organic components can therefore be removed upon photochemical conversion of the precursor films, leading to the formation of tin(II) oxide films. These properties make tin(II) 2-ethylhexanoate a suitable material for UV-NIL.

Images a and b in in Figure 4 are SEM and AFM images of the first replicated PUA mold and the first imprinted pattern. The line dimensions and grating pitch were successfully replicated, using photosensitive tin(II) 2-ethylhexanoate by UV-NIL. To reduce the line dimensions, samples of the first imprinted pattern were annealed at different temperatures. The widths of the imprinted lines, annealed at 200, 300, 400, and 500 °C for 1 h were 160, 140, 90, and 90 nm, whereas the heights of those were 300, 250, 170, and 160 nm, respectively. Therefore, annealing led to a significant reduction in line width and height. XRD characterization indicated that a UV-irradiated film is amorphous and remains amorphous up to 300 °C annealing (see the Supporting Information, Figure S1). Upon annealing at 400 °C for 1 h, a nanocrystalline film was obtained. The diffraction peaks of the nanocrystalline phase were found to correspond to those from crystalline SnO_2. Therefore, annealing an irradiated film at 400 °C in air resulted in the

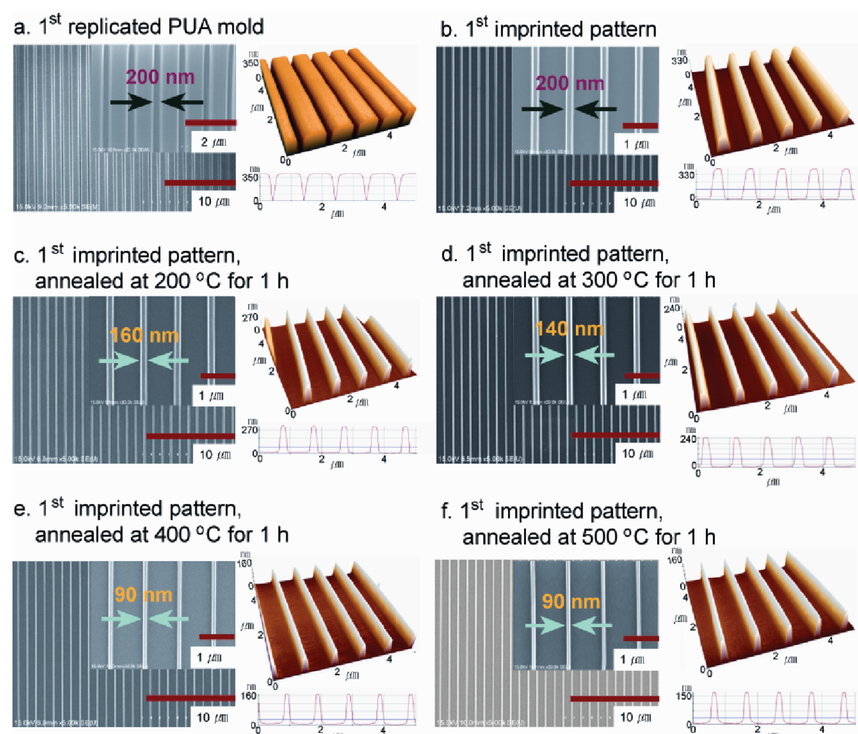

Figure 4. (a) SEM and AFM images of the 1st replicated PUA mold with trenches of 200 nm wide and 400 nm high at a pitch of 1000 nm. (b) SEM and AFM images of the 1st imprinted pattern and the pattern annealed at (c) 200, (d) 300, (e) 400, and (f) 500 °C for 1 h, respectively.

oxidation of amorphous tin(II) oxide and the formation of nanocrystalline SnO_2. Higher annealing temperatures improved crystallinity of the film.

With annealing, the volume reduction of the imprinted lines could be originated from the elimination of trapped organic molecules inside the film, densification of material, and structural arrangement for the formation of nanocrystalline phase. A summary can be found in Table 2 for the percentage dimension reduction in the line width and height at different annealing temperatures. It can be seen that the percentage dimension loss in line width is always less than that in line height, which could be related to the lateral confinement due to the material's adhesion to the substrate. Interestingly, the dimension loss in the line width and height between 300 and 400 °C was found to be higher than that resulted from lower annealing temperatures. Presumably, at lower annealing temperatures, the oxidation of tin(II) oxide, which is expected to cause an increase of material volume, partially compensates the volume reduction caused by material densification. It has been reported that tin(II) oxide might be oxidized at as low as 80 °C.[31] At annealing temperatures between 300 and 400 °C, the oxidation of tin(II) oxide might approach to completion and there would be no more compensation for the volume reduction caused now predominantly by material densification and crystal growth. Annealing at 500 °C resulted in a slightly further dimension loss, indicating that the SnO_2 film probably approaches to its best achievable density at 400 °C and further increase of crystallite size by higher annealing temperatures does not involve substantial volume change. Therefore, 400 °C is considered as the optimal annealing temperature for our size reduction lithography.

Table 2. Feature Size Reduction in the Lateral and Vertical Directions for the Imprinted Patterns Annealed at Different Annealing Temperatures

	lateral dimension		vertical dimension	
annealing conditions	line width (nm)	reduction in width (%)	line height (nm)	reduction in height (%)
no annealing	200		400	
annealing at 200 °C	160	20.0	300	25.0
annealing at 300 °C	140	30.0	250	37.5
annealing at 400 °C	90	55.0	170	57.5
annealing at 500 °C	90	55.0	160	60.0

To fabricate sub 50-nm SnO_2 lines, the PUA mold fabrication and the metal−organic compound imprinting and annealing processes were repeated, using the first imprinted pattern annealed at 400 °C as a new master. As shown in Figure 5a, the structures on the new master were replicated onto a PUA mold as a second replicated PUA mold. A second imprinted pattern was prepared from tin(II) 2-ethylhexanoate using the second replicated PUA mold, followed by annealing at 400 °C for 1 h. The line width and height of this sample were measured to be 40 and 50 nm, respectively. These correspond to 55.6% and 68.8% dimension loss in line width and height, similar to the dimension loss achieved by annealing the first imprinted pattern at 400 °C. Therefore, by performing our size reduction lithography twice, the obtained SnO_2 lines have width and height that were reduced totally by 80 and 87.5%, respectively, from the line dimensions available on the original Si master. Still, further size reduction is possible by repeating the above-described size reduction lithography multiple times. Despite the significant shrinkage, macroscopically uniform and

dx.doi.org/10.1021/am300203g | ACS Appl. Mater. Interfaces 2012, 4, 2507−2514

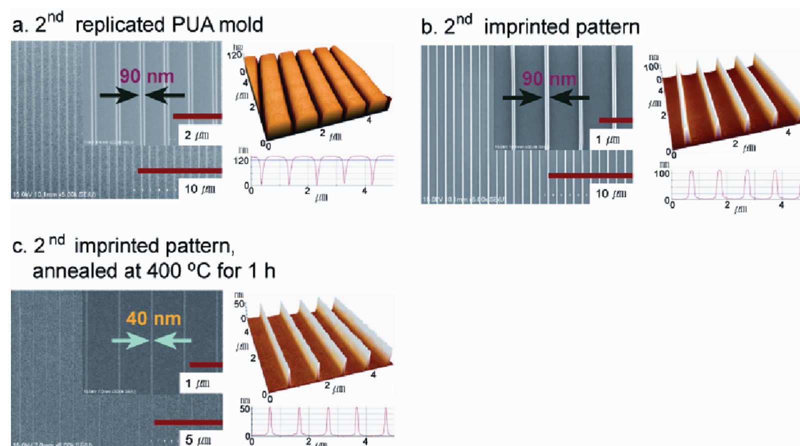

Figure 5. (a) SEM and AFM images of a 2nd replicated PUA mold. (b) SEM and AFM images of the 2nd imprinted pattern and (c) the pattern annealed at 400 °C for 1 h.

crack-free SnO_2 nanostructures were obtained on 4 in. wafers with good repeatability.

The optical band gap (E_g), optical transmittance, and refractive index (see Supporting Information, Figure S2) of various films prepared from tin(II) 2-ethylhexanoate were also studied. The optical absorption coefficient α of a semiconductor close to the band edge can be expressed by the following equation:[32]

$$\alpha h\nu = \kappa(h\nu - E_g)^n \quad (2)$$

where κ is a constant, E_g is the optical band gap (eV), and n is a value that depends on the nature of the transition. In this case, n is equal to 1/2 for the direct allowed transition. The optical band gap of a semiconductor can be estimated from a plot of $(\alpha h\nu)^2$ versus photon energy. Shown in Figure 6a are the plots of $(\alpha h\nu)^2$ versus photon energy for the precursor film, the irradiated film, and the films annealed at various temperatures. The optical band gaps for various films are indicated by the dashed lines. Compared to a precursor film, the optical band gap of the UV-irradiated film is red-shifted from 5.00 to 4.88 eV. Upon annealing, the band gaps are red-shifted even more. This red-shift trend can be explained as follows.

The precursor film consists of tin(II) 2-ethylhexanoate and each precursor molecule can be considered as a tin(II) oxide center surrounded by organic groups. The presence of bulky organic groups creates barriers between tin(II) oxide particles, resulting in a large band gap due to quantum confinement. During photolysis, an increasing number of bulky organic groups left the film and tin(II) oxide particles had greater opportunities to associate into larger particles as the irradiation proceeded. As a result of the growth of tin(II) oxide particles in the film, the E_g of the irradiated film appeared to be red-shifted. The introduction of annealing at 300 °C led to oxidation of tin(II) oxide, resulting in the formation of SnO_2 particles and promoting the association between SnO_2. This led to a large red-shift from 4.88 to 4.45 eV. At higher annealing temperatures, the film is converted from amorphous to crystalline phase and SnO_2 crystals grew into larger sizes, leading to a further red-shift in band gap. The E_g of the film annealed at 600 °C is 3.90 eV, approaching the E_g of bulk SnO_2 (3.60 eV).[33] Using the Scherrer equation and XRD data, the average nanocrystallite sizes for the films annealed at 400, 500, and 600 °C for 1 h were calculated to be 3, 5, and 8 nm, respectively (see the Supporting Information, Figure S1). It is well-known that quantum confinement (QC) can occur in semiconducting nanostructures and that QC converts the continuous-band structure to discrete electronic levels and results in the increase

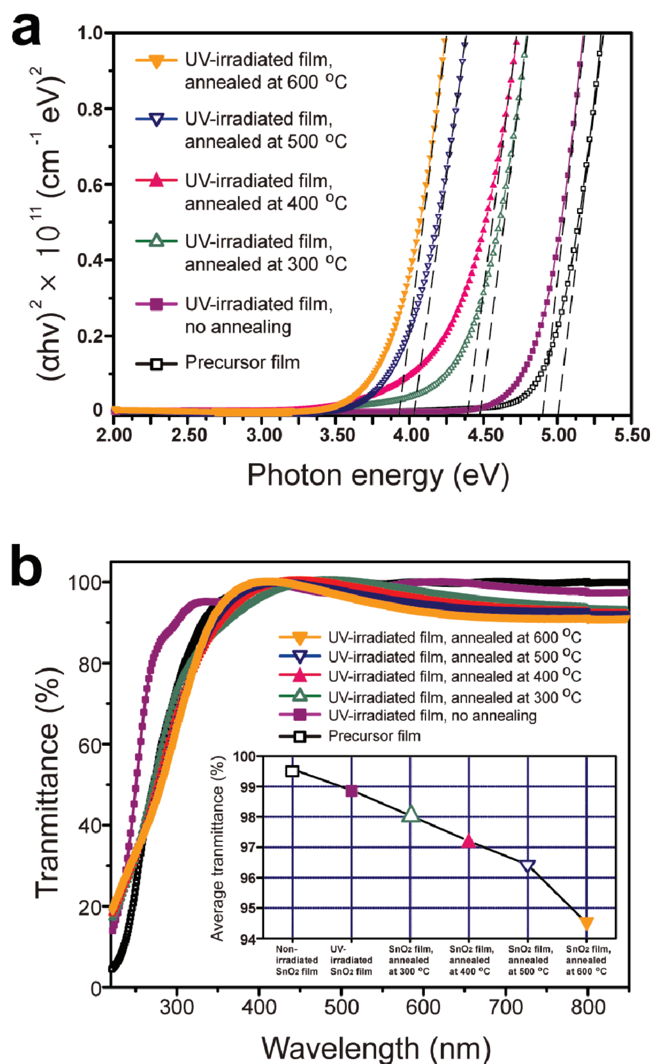

Figure 6. (a) Optical band gap and (b) optical transmittance obtained from the precursor film, the UV-irradiated film and the films annealed at 300, 400, 500, and 600 °C for 1 h, respectively.

in the band gaps with decreasing nanocrystallite sizes.[34] Souza et al. reported that the effect of QC for SnO_2 films is mainly considered in the size regime of several nanometers.[35] A similar increase in E_g with decreasing nanocrystallite size was also reported for SnO_2 nanocrystals.[36] Therefore, QC effect is presumably the main reason why the E_g of our films were all larger than that of bulk SnO_2 (3.60 eV).

Figure 6b shows the optical transmittance curves of various films prepared from tin(II) 2-ethylhexanoate on quartz substrates. As shown in the inset of Figure 6b, the increase in the annealing temperature resulted in a slight decrease of the average transmittance in the visible-light range of 400 to 700 nm. This slight reduction in the average transmittance might be due to the increase in the light scattering at the surface of SnO_2 film. During high-temperature annealing, crystallization of the amorphous film could lead to surface roughening. In addition, higher temperature could cause SnO_2 surface to generate defect states with oxygen deficiencies.[37] These defect states would increase optical absorbance of the annealed films. Nevertheless, the film annealed at 400 °C still demonstrated transmittance greater than 97% over the entire visible-light range and greater than 90% in the UV region from 350 to 400 nm. This makes the imprinted SnO_2 patterns also potentially useful as transparent molds for the UV-NIL process.

The electrical properties of the UV-irradiated films annealed at various temperatures were investigated by Hall measurements, and the results are given in Figure 7. The resistivity and

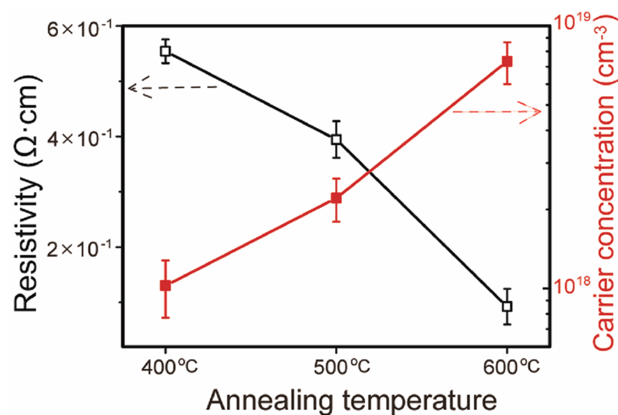

Figure 7. Resistivity (open squares) and carrier concentration (solid squares) of the UV-irradiated film as functions of annealing temperature.

carrier concentration of the films change strongly as functions of annealing temperature, particularly when the annealing temperature is above 500 °C. With increase of annealing temperature, the film resistivity decreases while the carrier concentration increases. The decrease in the resistivity and the increase of the carrier concentration can be interpreted as results of improved film quality. As previously discussed, higher annealing temperatures lead to increased grain sizes, which reduce the carrier scattering at grain boundaries, thereby giving rise to decreased resistivity and increased carrier concentration.

For applications of TCOs, the oxide is required to possess a band gap of 3.1 eV or more in order to transmit at least 85% visible light and a carrier concentration greater than 2.6×10^{21} cm^{-3}.[38,39] In our case, the optical transmittance and carrier concentration of the film annealed at 600 °C were approximately 94% and 7.32×10^{18} cm^{-3}, respectively. These values, together with the 40 nm patterning capability, make our UV-NIL SnO_2 films a potential candidate to transparent interconnects in applications such as light emitting diodes, solar cells, and optoelectronic devices. It will be an interesting area of future work to investigate how electrical properties of functional SnO_2 materials can be further improved by incorporating various dopants and/or metal nanomaterials.

CONCLUSION

We have demonstrated a new method of size reduction lithography based on UV-NIL, where the polymer PUA replication and inorganic imprinting and annealing processes are used sequentially and repeatedly, in order to obtain smaller feature sizes. The feature size of imprinted patterns can be controllably reduced by varying the annealing temperature and repeating the size reduction lithography multiple times. The photochemical reaction of tin(II) 2-ethylhexanoate was studied and a reaction mechanism was postulated. It was found that tin(II) 2-ethylhexanoate is a suitable precursor to fabricate SnO_2 patterns by UV-NIL. SnO_2 line structures of 40 nm wide and 50 nm high were obtained from a Si master with lines of 200 nm wide and 400 nm high, by simply performing size reduction lithography twice. This resulted in dimension loss of 80 and 87.5% in the line width and height, respectively. Despite this significant shrinkage, macroscopically uniform and crack-free SnO_2 patterns were obtained on 4 in. wafers. Through optical characterization, it was found that the SnO_2 film annealed at 400 °C still demonstrated transmittance greater than 90% over the range of 350 to 700 nm, making it also useful as molds in UV-NIL. Unlike the conventional UV-NIL method, the proposed technique offers a flexible way for the facile size-tunable fabrication of intermediate imprint masters (or molds), as well as the nanofabrication of functional oxide patterns.

ASSOCIATED CONTENT

Supporting Information

MS analysis of the volatile photoproducts formed by photolysis of a tin(II) 2-ethylhexanoate film. Structural investigation of UV-irradiated film and annealed films: X-ray diffraction spectra. Refractive index values of UV-irradiated film and annealed films. This material is available free of charge via the Internet at http://pubs.acs.org.

AUTHOR INFORMATION

Corresponding Author

*Address: Nano Process Division, Korea Advanced Nano Fab Center (KANC), 906-10, Iui-dong, Yeongtong-gu, Suwon-si, Gyeonggi-do, 443-270, Republic of Korea. Telephone: +82-31-546-6312. Fax: +82-31-546-6409. E-mail: hokwan.kang@kanc.re.kr.

Present Address

[§]Technology Transfer Center, The Hong Kong University of Science and Technology, Clear Water Bay, Kowloon, Hong Kong, China

Notes

The authors declare no competing financial interest.

ACKNOWLEDGMENTS

This research was supported by a grant from Gyeonggi Technology Development Program funded by Gyeonggi Province.

REFERENCES

(1) Wanke, M. C.; Lehmann, O.; Muller, K.; Wen, Q. Z.; Stuke, M. *Science* **1997**, *275*, 1284−1286.
(2) Poborechii, V. V.; Tada, T.; Kanayama, T. *Appl. Phys. Lett.* **1999**, *75*, 3276−3278.
(3) Haes, A. J.; Van Duyne, R. P. *J. Am. Chem. Soc.* **2002**, *124*, 10596−10604.
(4) Lee, K. B.; Park, S. J.; Mirkin, C. A.; Smith, J. C.; Mrksich, M. *Science* **2002**, *295*, 1702−1705.
(5) Cui, Y.; Wei, Q. Q.; Park, H. K.; Lieber, C. M. *Science* **2001**, *293*, 1289−1292.
(6) Grunes, J.; Zhu, J.; Somorjai, C. A. *Chem. Commun.* **2003**, 2257−2260.
(7) Matsui, S.; Ochiai, Y. *Nanotechnology* **1996**, *7*, 247−258.
(8) Park, H.-H.; Lee, H.-S.; Park, H.-H.; Zhang, X.; Hill, R. H. *J. Electrocerm.* **2010**, *24*, 214−218.
(9) Shir, D.; Yoon, J.; Chanda, D.; Ryu, J.-H.; Rogers, J. A. *Nano Lett.* **2010**, *10*, 3041−3046.
(10) Gao, H.; Tan, H.; Zhang, W.; Morton, K.; Chou, S. Y. *Nano Lett.* **2006**, *6*, 2438−2441.
(11) Oda, H.; Ohtake, T.; Takaoka, T.; Nakagawa, M. *Langmuir* **2009**, *25*, 6604−6606.
(12) Choi, Y.-K.; King, T.-J.; Hu, C. *Solid-State Electron.* **2002**, *46*, 1595−1601.
(13) Low, H. Y.; Chong, K. S. L. *Langmuir* **2009**, *25*, 6559−6564.
(14) Park, H.-H.; Zhang, X.; Lee, S.-W.; Kim, K.-D.; Choi, D.-G.; Choi, J.-H.; Lee, J.; Lee, E.-S.; Park, H.-H.; Hill, R. H.; Jeong, J.-H. *J. Mater. Chem.* **2011**, *21*, 657−662.
(15) Wang, Q.; Zhang, L.-S.; Wu, J.-F.; Wang, W. D.; Song, W.-G.; Wang, W. *J. Phys. Chem. C* **2010**, *114*, 22671−22676.
(16) Park, S.-S.; Mackenzie, J. D. *Thin Solid Films* **1995**, *258*, 268−273.
(17) Candeloro, P.; Comini, E.; Baratto, C.; Faglia, G.; Sberveglieri, G.; Kumar, R.; Carpentiero, A.; Fabrizio, E. D. *J. Vac. Sci. Technol. B* **2005**, *23*, 2784−2788.
(18) Jiang, L.-Y.; Wu, X.-L.; Guo, Y.-G.; Wan, L.-J. *J. Phys. Chem. C* **2009**, *113*, 14213−14219.
(19) Wang, Y.; Gao, G. *Adv. Mater.* **2008**, *20*, 2251−2269.
(20) Maier, J. *Nat. Mater.* **2005**, *4*, 805−815.
(21) Tamai, T.; Ichinose, N.; Kawanishi, S.; Nishii, M.; Sasuga, T.; Hashida, I.; Mizuno, K. *Chem. Mater.* **1997**, *9*, 2674−2675.
(22) Tadanaga, K.; Owan, T.; Morinaga, J.; Urbanek, S.; Minami, T. *J. Sol−Gel Sci. Technol.* **2000**, *19*, 791−794.
(23) Choi, S. J.; Yoo, P. J.; Beak, S. J.; Kim, T. W.; Lee, H. H. *J. Am. Chem. Soc.* **2004**, *126*, 7744−7745.
(24) Seo, S.-M.; Kim, T.-I.; Lee, H. H. *Microelectron. Eng.* **2007**, *84*, 567−572.
(25) Kim, J. Y.; Choi, D.-G.; Jeong, J.-H.; Lee, E.-S. *Appl. Surf. Sci.* **2008**, *254*, 4793−4796.
(26) Chang, S.-M.; Doong, R.-A. *Chem. Mater.* **2007**, *19*, 4804−4810.
(27) Zhu, H. J.; Hill, R. H. *J. Non-Cryst. Solids* **2002**, *311*, 174−184.
(28) Hill, R. H.; Blair, S. L. *ACS Symp. Ser.* **1998**, *706*, 53−66.
(29) Law, W. L. Ph.D. Dissertation. Simon Fraser University, Burnaby, BC, Canada, 2004.
(30) Park, H.-H.; Choi, D.-G.; Zhang, X.; Jeon, S.; Park, S.-J.; Lee, S.-W.; Kim, S.; Kim, K.-D.; Choi, J.-H.; Lee, J.; Yun, D. K.; Lee, K. J.; Park, H.-H.; Hill, R. H.; Jeong, J.-H. *J. Mater. Chem.* **2010**, *20*, 1921−1926.
(31) Macías, M. A.; Martínez, J. A. H.; Gauthier, G. H.; Rodriguez, J. E.; Avila, H.; Pinto, J.; Pinilla, J. *Mater. Res.* **2011**, *14*, 172−177.
(32) Kar, A.; Patra, A. *J. Phys. Chem. C* **2009**, *113*, 4375−4380.
(33) Yadav, J. B.; Patil, R. B.; Puri, R. K.; Puri, V. *Mater. Sci. Eng., B* **2007**, *139*, 69−73.
(34) Liu, F. X.; Yang, J. L.; Zhao, T. P. *Phys. Rev. B* **1997**, *55*, 8847−8851.
(35) Souza, A. E. D.; Monteiro, S. H.; Santilli, C. V.; Pulcinelli, S. H. *J. Mater. Sci.* **1997**, *8*, 265−270.
(36) He, Y.; Liu, J. F.; Chen, W.; Wang, Y.; Wang, H.; Zeng, Y. W.; Zhang, G. Q.; Wang, L. N.; Liu, J.; Hu, T. D.; Hahn, H.; Gleiter, H.; Jiang, J. Z. *Phys. Rev. B* **2005**, *72*, 212102.
(37) Maestre, D.; Cremades, A.; Piqueras, J. *Semicond. Sci. Technol.* **2004**, *19*, 1236−1239.
(38) Hamberg, I.; Granqvist, C. G. *J. Appl. Phys.* **1986**, *60*, R123−R159.
(39) Hoel, C. A.; Mason, T. O.; Gaillard, J.-F.; Poeppelmeier, K. R. *Chem. Mater.* **2010**, *22*, 3569−3579.